Building and Environment 93 (2015) 86–96

Contents lists available at ScienceDirect

Building and Environment

journal homepage: www.elsevier.com/locate/buildenv

Enhanced spread of expiratory droplets by turbulence in a cough jet

Jianjian Wei*, Yuguo Li

Department of Mechanical Engineering, The University of Hong Kong, Pokfulam Road, Hong Kong

ARTICLE INFO

Article history:
Received 14 April 2015
Received in revised form
5 June 2015
Accepted 17 June 2015
Available online 20 June 2015

Keywords:
Turbulent cough jets
Expiratory droplets
Particle tracking model
Evaporation
Dispersion

ABSTRACT

Coughing has been confirmed as a significant vector for transmitting respiratory diseases. It can be modelled physically as a turbulent jet to study the dispersion of expiratory droplets. The discrete random walk model for particle tracking is employed to study the effect of turbulence fluctuation on dispersion of particles and/or droplets. The concept of reach probability is proposed to characterise the streamwise spread distance. Our study shows that jet-like cough airflow turbulence prompts the wide spread of particles and expiratory droplets, and that the effect of evaporation on medium droplets (50 μm) is most significant. When turbulence fluctuations are considered for the 100 μm particles, there is a four-fold increase in the dispersion range in the streamwise direction, and a thirteen-fold increase in the transverse direction compared to that without fluctuation. Small particles are found to follow the airflow closely, dispersing in the whole jet region, while only 1% of large particles exceed 2 m in the streamwise direction; nearly 10% of medium particles travel 4.0 m (initial $u_0 = 10$ m/s, mouth diameter $D = 2$ cm). Droplets evaporate after being exhaled, but fates of small droplets with initial diameter $d_{p0} = 30\mu m$ as well as large droplets with $d_{p0} = 100\mu m$ are little affected by relative humidity (RH). The 30 μm droplets evaporate in seconds and behave similarly to the 10 μm particles. The spread distance of large droplets is mainly determined by the jet outlet diameter and velocity. In contrast, the medium droplets are found to be very sensitive to RH under humid conditions (RH ≥ 80%).

1. Introduction

Many respiratory diseases can be transmitted via direct spray of droplets, long- and short-range airborne routes, and/or by indirect contact. The precise transmission mode(s) for some diseases remains controversial, e.g. influenza. The literature review by Brankston et al. [1] concluded that influenza infection generally occurs over short rather than long distances. On the other hand, a literature review by Tellier [2], concluded that aerosol transmission occurs at considerable rates, while Weber & Stilianakis [3] found contact, large droplet and small droplet (aerosol) transmission all to be potentially important modes of transmission for the influenza virus. These in-depth reviews also revealed the importance of studying exposure of expiratory droplets/droplet nuclei among people, as it is a prerequisite for transmission of respiratory diseases.

The formation mechanisms of expiratory droplets have been studied, including the instability and break up of mucus during coughing and sneezing [4–6], and rupture of liquid film at thermal airways [7,8]. A number of droplet generation measurements have found that the majority of exhaled droplets during breathing are in the sub-micron range, while coughing and sneezing can produce large droplets [7,9–13]. Wells [14] first defined large droplets as those over 100 μm in aerodynamic diameter. The mechanism of droplet formation and origin is also associated with virus and bacteria load in droplets, as pathogens are usually limited to certain areas of the body [7]. Lindsley et al. [15] used the quantitative polymerase chain reaction (qPCR) to measure the influenza virus in aerosol particles from human coughs. Some 35% of the detected influenza RNA was contained in particles >4 μm in diameter, 23% in particles of 1–4 μm, and 42% in particles <1 μm, showing not only that coughing by patients emits aerosols containing the influenza virus, but also that much of the viral RNA is contained within particles in the respirable size range.

The fate of expiratory droplets in the indoor environment, or more specifically, how far they travel, is associated with exposure and subsequent infection/disease. The travel distance and dispersion of droplets is itself a complex phenomenon, which is affected by the sub-micron-scale evaporation of droplets [16–18], room ventilation and obstacles [19–21], thermal plume around and

* Corresponding author.
E-mail address: wei.jianjian.88@gmail.com (J. Wei).

http://dx.doi.org/10.1016/j.buildenv.2015.06.018
0360-1323/

above a person [22–24], and human conversational behaviour and activities [25–27], etc. However, droplet size seems the most important factor affecting dispersion and deposition [7]. The airflow in buildings is designed to be less than 0.25 m/s for thermal comfort [28]. The jet speed of coughing and breathing can be 6–22 m/s (over 10 m/s on average) and 1–5 m/s respectively [13,29,30]. The transport of the expiratory droplets can be considered as two stages, with the primary being coughing/exhalation jet transport, followed by the secondary, dispersion by room airflow.

Among all respiratory activities, coughing has probably been studied the most due to its significance in disease transmission. Its high-velocity airflow can induce instability at the mucous–air interface, and droplets generated due to the instability mechanism can be carried a long distance by airflow after being expelled from the human respiratory tract [31]. The number of droplets during a single cough can be as high as 3000 [9]. The maximum coughing airflow velocity at the mouth has been measured in the order of 10 m/s [13,29,32]. The Schlieren technique using human volunteers reveals the turbulent cough jet with a leading vortex [33], with similar properties to a jet or puff [34]. Trajectories of large droplets from coughing and sneezing were recently visualised by Bourouiba and Bush [35]. Wells [14] developed an evaporation–deposition curve of droplets, and distinguished the airborne and droplet transmission. Xie et al. [36] extended the study by analysing the cough jet as a steady round jet, and found that the expired droplets can travel up to 1.5–2 m. The effect of turbulence was not considered. Most computer modelling studies also have not properly considered the impact of turbulence. Klettner et al. [37] theoretically demonstrated that the effect of turbulence significantly increases the transmission distance and spread of droplets in a hospital room. The effect of turbulence on particle dispersion in jets has been investigated in related disciplines such as hydraulics [38–40] and combustion [41].

Spread of espiratory dropletjets in a turbulent steady cough jet will be systematically investigated. Our hypothesis is that turbulence can enhance the dispersion and spread of expired droplets, and such a wide spread has significant implications for disease transmission between people. In this paper, we employ a well-established particle tracking model, i.e. the discrete random walk model (DRW), to study the effect of turbulence on dispersion and deposition of particles and droplets in a cough jet. The effect of evaporation of droplets is investigated. The ambient air is assumed to be stagnant, which offers an ideal situation to study the spread of droplets due to the cough jet alone.

2. Mathematical models

The investigated scenario is illustrated in Fig. 1. We propose an analytical approach instead of computational fluid dynamics (CFD) analysis. The advantage of such an approach lies in offering good physical insight into the droplet spread. We model the detailed processes of cough jet flow, including droplet evaporation and motion, turbulent round jet, and particle tracking, to study the dispersion and deposition of expiratory droplets in a room during coughing.

2.1. Particle motion equation

Particles are non-evaporative, while droplets shrink by evaporation, but we treat both droplets and particles as rigid spheres in solving their motion equation. The trajectories of particles and droplets are determined using a Lagrangian formulation of the governing equations. In our situation $\rho_p/\rho_g > 800$, so we ignore the effects of virtual mass, Basset history force and Magnus force, and particle collision are also ignored in the dilute particle-laden flows. The motion equation is given by

$$\frac{d\mathbf{u}_p}{dt} = \frac{3\rho_g C_D}{4 d_p \rho_p}(\mathbf{u}_g - \mathbf{u}_p)|\mathbf{u}_g - \mathbf{u}_p| + \mathbf{g} \ \text{(a)} \qquad \frac{d\mathbf{x}_p}{dt} = \mathbf{u}_p \ \text{(b)} \tag{1}$$

where subscripts g and p denote gas and particles, respectively; u is the velocity, ρ is the density, d_p is the particle diameter, C_D is the drag coefficient, and g is the gravitational acceleration.

The drag coefficient is determined from the following correlation:

$$C_D = \begin{cases} \dfrac{24}{\mathrm{Re}}, & \mathrm{Re} \le 1 \\ \dfrac{24}{\mathrm{Re}}\left(1 + 0.15\mathrm{Re}^{0.687}\right), & \mathrm{Re} > 1 \end{cases} \tag{2}$$

with Reynolds number $\mathrm{Re} = \dfrac{|\boldsymbol{u}_p - \boldsymbol{u}_g| d_p}{\nu}$

2.2. Evaporation of a single droplet

Heat and mass transfer occur simultaneously at the droplet surface after they are exhaled into air. Droplets are assumed to remain spherical, and the temperature is uniform inside the droplets. The mass flux was given by Kukkonen et al. [42].

$$-\frac{dm_p}{dt} = I_v = -\frac{2\pi p d_p M_w D_\infty C_T \mathrm{Sh}}{R T_\infty} \ln\left(\frac{p - p_{vs}}{p - p_{v\infty}}\right) \tag{3}$$

where M_w is the molecular weight of water vapour, D_∞ the binary diffusion coefficient far from the droplet, R the universal gas constant, p the total pressure, p_{vs} the vapour pressure at the droplet surface and $p_{v\infty}$ the vapour pressure distant from it,$C_T = \frac{T_\infty - T_p}{T_\infty^{\lambda-1}} \frac{2-\lambda}{T_\infty^{2-\lambda} - T_p^{2-\lambda}}$ (λ is a constant between 1.6 and 2) is a correction factor because of the temperature dependence of the diffusion coefficient. The Sherwood number $\mathrm{Sh} = 1 + 0.38\mathrm{Re}^{1/2}\mathrm{Sc}^{1/3}$ accounts for the enhanced mass transfer rate by convective effect.

The heat transfer through the droplet surface is described by

$$(m_l C_l + m_s C_s)\frac{dT_p}{dt} = \pi d_p^2 K_g \frac{T_\infty - T_p}{r_p}\mathrm{Nu} - L_v I_v \tag{4}$$

where m_l and m_s are the mass of liquid and solid parts of the droplet, respectively, the specific heat C_l and C_s are assumed to be that of the pure water and 1000 J/(kg·K), respectively, K_g the thermal conductivity of air, L_v the latent heat of vaporisation, Nusselt number $\mathrm{Nu} = 1 + 0.3\mathrm{Re}^{1/2}\mathrm{Pr}^{1/3}$.

We consider both the Kelvin effect - a higher partial vapour pressure on the droplet surface due to the curvature of droplet surface, and the solute effect - a lower partial vapour pressure by the non-volatile solutes, to obtain the partial vapour pressure at the droplet surface [17].

$$\ln\frac{p_{va}}{p_{sat}} = \ln a_w + \frac{4M_w\sigma_{LV}}{\rho_w R T_\infty d_e} = -\frac{\gamma \Psi_{salt} M_w c_i (1 - \Phi_i)}{M_{salt}(1 - c_i)} \frac{1}{(d_p/d_{p0})^3 - \Phi_i} + \frac{4M_w\sigma_{LV}}{\rho_w R T_\infty d_p} \tag{5}$$

where a_w is the water activity, γ is the total number of ions a salt molecule dissociates into ($\gamma = 2$ for NaCl), Ψ_{salt} the practical osmotic coefficient as a function of the salt concentration ($\Psi_{salt} = 1.2$ here), Φ_i the initial insoluble solid volume ratio, c_i the NaCl

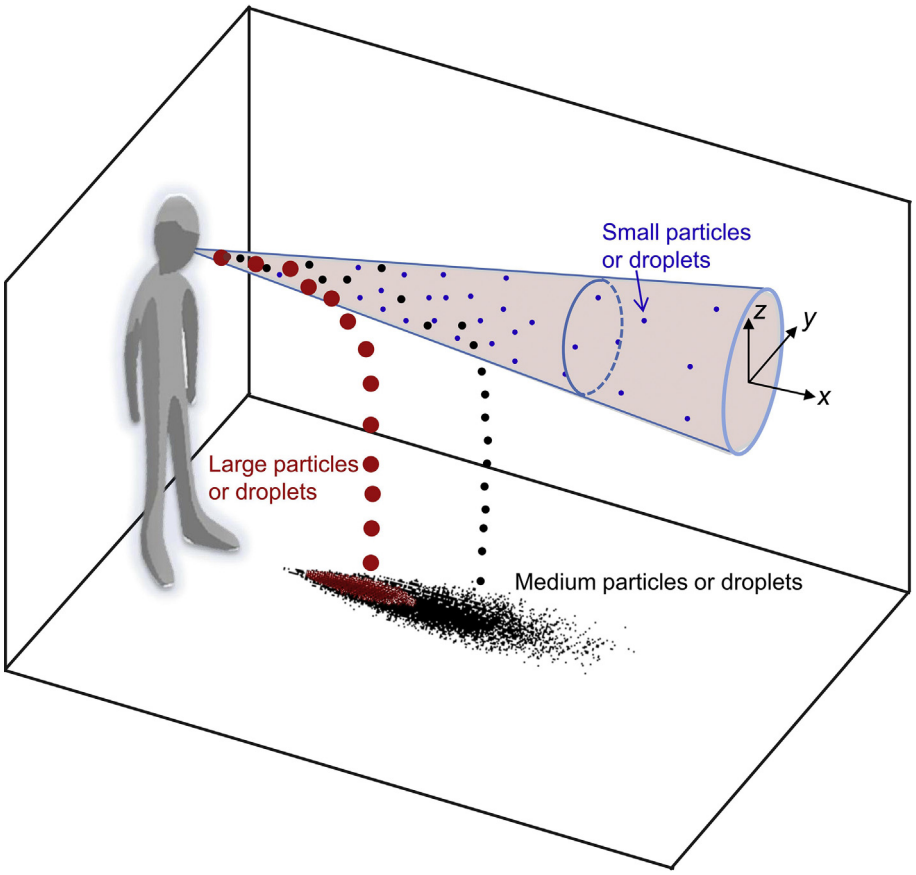

Fig. 1. Illustration of the investigated scenario. Three sizes of particles or droplets are released in a turbulent round cough jet.

concentration,d_{p0} the initial droplet diameter, M_{salt} the molecular weight of NaCl, and σ_{LV} the surface tension.

In this study, the initial solid volume ratio,Φ_i, is 1.8% following Duguid [9]; it is assumed to have the same density as water, and the initial NaCl concentration is 0.9%. In dry air droplets evaporate to their droplet nuclei sizes d_{pc}. It is determined by the solid residue formed by the insoluble solids, which are not compact inside the solid residue [44].

$$d_{pc} = \left(\frac{\Phi_i}{\psi_{max}}\right)^{1/3} d_{p0} \tag{6}$$

where $\psi_{max} = 0.5236$ is the maximum solid volume ratio inside the solid residue after the nuclei is formed.

In humid conditions, equilibrium is reached when $p_{vs} = p_{v\infty}$. In our case the threshold RH is about 67% [17]. The droplet nuclei would have a larger size than the crust diameter d_{pc} when RH is greater than 67%.

Typical properties of the particles and droplets are summarised in Table 1.

2.3. The turbulent round jet model

The turbulent jet theory is relatively well established [45–47]. For a free jet, there are two regions along the streamwise direction, i.e. the transitional region consisting of a potential core and a mixing layer, and the main region.

The jet mean streamwise velocity u_r and transverse velocity v_r are given by Refs. [39,46].

$$\frac{u_c}{u_0} = 6.2\left(\frac{x}{D}\right)^{-1} \tag{7}$$

$$\frac{u_r}{u_c} = \exp\left(-\frac{r^2}{b^2}\right) \tag{8}$$

$$\frac{v_r}{\alpha u_c} = \frac{1-\exp(-r^2/b^2)-(\beta/\alpha)(r^2/b^2)\exp(-r^2/b^2)}{r/b} \tag{9}$$

where u_0^2 is the initial velocity of the jet, u_c is the mean centreline velocity, u_r is the mean streamwise velocity and v_r is the mean transverse velocity; $b = \beta x$ is the Gaussian half width and $\beta = 0.114$; $u_e = a u_c$ is the entrainment velocity at $r = b$; $\alpha = 0.057$ is the jet entrainment coefficient. The visual boundary of the jet corresponds to a jet velocity distribution represented by a simplified top-hat profile that preserves the same mass and momentum fluxes with that of a Gaussian profile (Fig. 2); the top-hat width $b_t = \sqrt{2}b = 0.16x$.

Note that our jet flow model considers both the air flow in the jet, as well as in the surrounding areas (Fig. 2).

The semi-empirical root mean square turbulent velocity fluctuation and turbulent dissipation rate profiles derived from CFD modelling are as follows [40].

$$\frac{\sigma(r)}{u_c} = C_1\left[\exp\left(-C_2\left(\frac{r}{b}-C_3\right)^2\right)+\exp\left(-C_2\left(\frac{r}{b}+C_3\right)^2\right)\right] \tag{10}$$

Table 1
Characteristic parameters of particles or expiratory droplets of typical sizes. (w_s is the terminal settling velocity, τ relaxation time, S stopping distance [43], t_{2m} time to fall 2 m, t_{dry} time for droplets to become nuclei, d_{1s} is the size at one second after release and d_{pc} is the eventual respiratory droplet nuclei size. Re_0 and S are calculated with initial speed of $u_{p0} = 10$ m/s in stagnant air.) Air temperature is 25 °C for all calculations.

		Particle or droplet diameter d_{p0} (μm)							
		1	2	5	10	20	50	100	1000
Particle properties	w_s(mm/s)	0.03	0.12	0.74	2.96	11.8	74.0	245.7	3872
	τ (ms)	3.0×10^{-3}	0.012	0.076	0.30	1.21	7.6	25.1	395.1
	Re_0	0.644	1.29	3.22	6.44	12.9	32.2	64.4	644
	S (m)	3.0×10^{-5}	1.1×10^{-4}	6.2×10^{-4}	2.3×10^{-3}	8.0×10^{-3}	0.040	0.13	4.62
	t_{2m} (s)	6.76×10^{4}	1.69×10^{4}	2.70×10^{3}	675.7	168.9	27.0	8.1	0.52
Droplet properties	t_{dry} (RH = 0%) (s)	6.0×10^{-4}	2.5×10^{-3}	0.016	0.066	0.26	1.66	6.63	664.3
	t_{dry} (RH = 90%) (s)	3.1×10^{-3}	0.027	0.31	1.52	7.10	46.3	199.0	18382
	d_{1s} (RH = 0%) (μm)	0.325	0.650	1.63	3.25	6.50	33.5	92.4	998.2
	d_{1s} (RH = 90%) (μm)	0.325	0.673	1.89	4.02	17.2	48.9	99.4	999.8
	d_{pc} (RH < 67%) (μm)	0.325	0.650	1.63	3.25	6.50	16.3	32.5	325

$$\frac{(\varepsilon(r)b)^{1/3}}{u_c} = C_4\left[\exp\left(-C_5\left(\frac{r}{b}-C_6\right)^2\right)+\exp\left(-C_5\left(\frac{r}{b}+C_6\right)^2\right)\right] \tag{11}$$

where $C_1 = 0.2006$, $C_2 = 1.4147$, $C_3 = 0.6647$, $C_4 = 0.2458$, $C_5 = 1.2498$ and $C_6 = 0.6594$.

For non-isothermal jets, the centreline is curved, and the trajectory of the centreline of a horizontally projected circular jet can be estimated as follows [45].

$$\frac{z}{\sqrt{A_0}} = 0.0354\mathrm{Ar}_0\left(\frac{y}{\sqrt{A_0}}\right)^3\sqrt{\frac{T_0}{T_\infty}} \tag{12}$$

where Ar_0 is the Archimedes number

$$\mathrm{Ar}_0 = \frac{g\sqrt{A_0}}{u_0^2}\frac{\Delta\rho}{\rho_0}$$

A_0 is the area of the supply opening, T_0 is the initial temperature of the jet, T_∞ is the temperature of ambient air (outside the jet), and $\Delta\rho = \rho_\infty - \rho_0$.

The thermal diffusion is more intense than momentum diffusion along the streamwise and transverse directions, which leads to a flatter temperature distribution than the velocity distribution. The following empirical equations for temperature T and water vapour density ρ_v decay of a non-isothermal jet [48] are applied in this study.

$$\frac{T_m - T_\infty}{T_0 - T_\infty} = \frac{\rho_{vm} - \rho_{v\infty}}{\rho_{v0} - \rho_{v\infty}} = \frac{5.0}{s}\sqrt{\frac{T_0}{T_\infty}} \tag{13}$$

$$\frac{T - T_\infty}{T_m - T_\infty} = \frac{\rho_v - \rho_{v\infty}}{\rho_{vm} - \rho_{v\infty}} = \exp\left[-\frac{r^2\ln 2}{(0.11s)^2}\right] \tag{14}$$

where T_m is the centreline temperature of the jet, ρ_{vm} is the water vapour density in the centreline of the jet, ρ_{v0} is the initial water vapour density of the jet and $\rho_{v\infty}$ is the water vapour density in the ambient air, and s the distance of the jet centreline travelled from the origin.

2.4. Particle tracking model

The instantaneous air velocity contains the mean velocity and its fluctuation,

$$u = \overline{u} + u' \tag{15}$$

The instantaneous air velocity is estimated to predict particle dispersion due to turbulence. One of the widely-used methods for

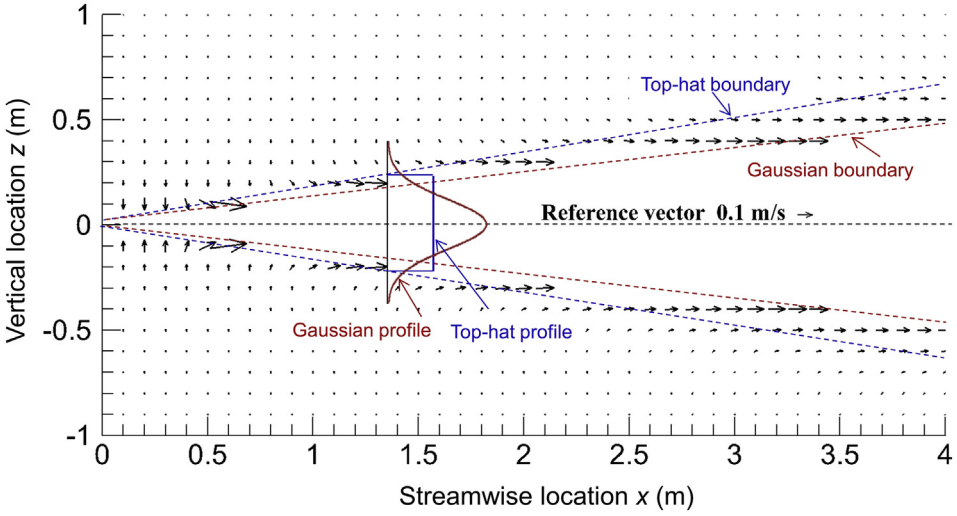

Fig. 2. The velocity distribution in the jet surrounding region (opening diameter $D = 2$ cm, initial velocity $u_0 = 10$ m/s; vector type: anchor at midpoint). The jet Gaussian boundary and top-hat boundary are shown by dashed lines, and the streamwise velocity profiles are shown by bold lines.

prediction particle dispersion in turbulent flows is the eddy interaction model or DRW model, originally proposed by Gosman and Ioannides [41]. The DRW model has been used in a number of studies of exhaled droplet dispersion in rooms; e.g. Chao and Wan [49]. The fluctuating velocity components are discrete piecewise constant functions of time, and their random value is kept constant over an interval of time, which is the minimum of either the eddy lifetime (t_e) or the transit time required for the particle to cross the eddy (t_r).

$$t_{\text{int}} = \min(t_e, t_r) \tag{16}$$

$$t_e = 2t_L = 2C_L\frac{k}{\varepsilon} \tag{17}$$

$$t_r = -\tau' \ln\left(1.0 - \frac{l_e}{\tau'|\mathbf{u}_g - \mathbf{u}_p|}\right) \tag{18}$$

where t_{int} is the interaction time between particles and air, $t_L = C_L\frac{k}{\varepsilon}$ is the Lagrangian integral time scale, and $C_L \approx 0.15$ for the $k-\varepsilon$ model and its variants; τ' is the particle relaxation time, defined as $\tau' = \frac{4\rho_p d_p}{3\rho_g C_D|\mathbf{u_g}-\mathbf{u_p}|}$; $|\mathbf{u_g} - \mathbf{u_p}|$ is the magnitude of the relative velocity at the start of interaction; $l_e = \frac{C_\mu^{3/4}k^{3/2}}{\varepsilon}$ is the eddy length scale.

2.5. Assumptions in the calculations

The above models were solved numerically. For a typical cough jet, the initial velocity (u_0^2) was set at 10 m/s, and the equivalent diameter of the mouth outlet (D) was 2 cm [29]. The mouth opening area was almost constant during the cough period, at about 4±0.95 cm^2 for males and 3.37±1.4 cm^2 for females [29]. A recent study by Kwon et al. [30] showed that the average coughing velocity is 15.3 m/s for males, and 10.6 m/s for females.

In our numerical simulations of particles from a non-buoyant cough jet, we assumed that particles are continuously and isokinematically released from the mouth opening (nozzle). The nozzle was divided into 100 sub-regions equal in area, and each particle was released randomly from one of them. This ensured that particles were uniformly distributed at the nozzle outlet. The release velocity was in the streamwise direction only. Three particle diameters of 10 μm, 50 μm and 100 μm are investigated; in each case the trajectories were calculated for a total of 50,000 particles. One particle was released every 0.01 s from $t = 0$, and the total release duration was 500 s.

For the droplet study, the initial solid volume ratio in expiratory droplets was set to 1.8%, and the initial NaCl concentration was 0.9%, following Duguid [9]. In our numerical simulations of a buoyant cough jet, 5000 droplets were released, and three initial diameters of 30 μm, 50 μm, and 100 μm were investigated. One droplet was released every 0.01 s for 30 μm droplets from $t = 0$, 0.04 s for medium ($d_{p0} = 50\mu m$) and for large droplets ($d_{p0} = 100\mu m$). The total release duration was 50 s for the 30 μm droplets, and 200 s for the 50 μm and 100 μm droplets.

The quantitative analysis in the following context is based on the statistical results of 50,000 particles or 5000 droplets in each case; that is not affected by the release rate. Continuous release is to obtain the instantaneous distribution pattern of droplets (Fig. 9). For example, it takes almost 200 s for a medium droplet to deposit on the ground surface, while the shortest time for a small droplet to reach $x = 4$ m is about 10 s.

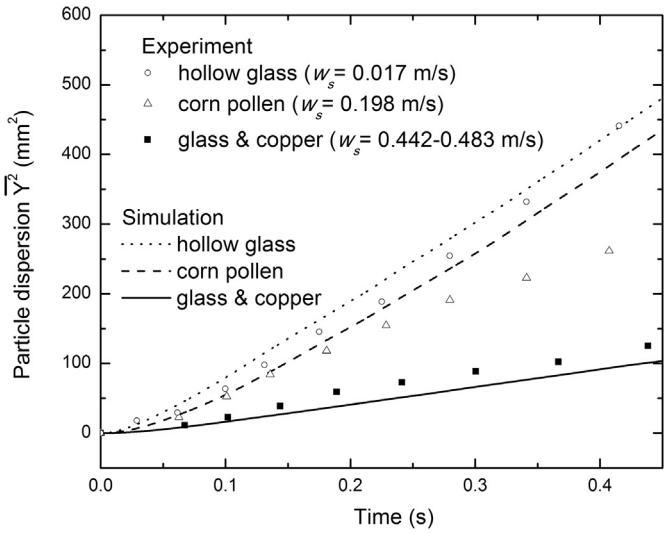

Fig. 3. Comparison of simulation results of the DRW model with the experimental data of Snyder and Lumley [50].

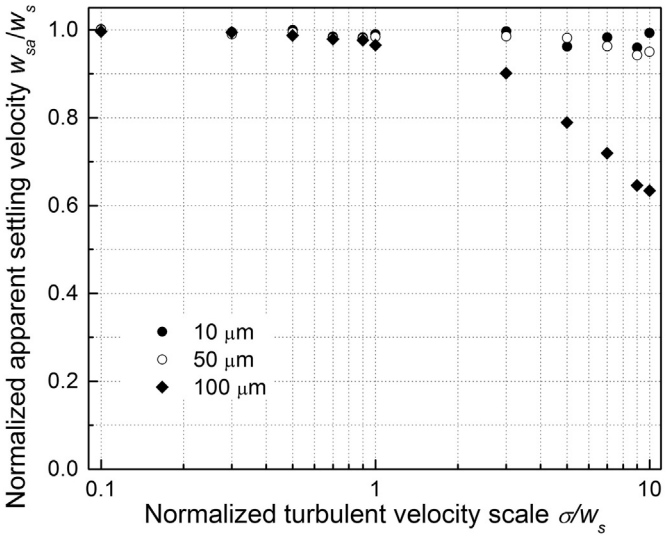

Fig. 4. Reduced particle settling velocity due to the existence of turbulence.

3. Results and discussions

The models were first validated, followed by their application to particle spread and deposition in a buoyancy-neutral round jet, and then for spread of droplets with the effect of evaporation. Note that in Sections 3.1–3.3, only particles are considered, i.e. we do not consider evaporation. The impact of evaporation on droplets is discussed in Sections 3.4–3.5.

3.1. Validation of the particle tracking model

The wind-tunnel experiment of Snyder and Lumley [50] was reproduced to validate the prediction of particle dispersion due to turbulence (Fig. 3). In the experiment, four types of particles (glass particles, $d_p = 87$ μm, $\rho_p = 2500$ kg/m^3; copper particles, $d_p = 46.5$ μm, $\rho_p = 8900$ kg/m^3; hollow glass, $d_p = 46.5$ μm, $\rho_p = 260$ kg/m^3; corn pollen, $d_p = 87$ μm, $\rho_p = 1000$ kg/m^3) were released isokinetically into the grid-generated turbulent flow in a vertical

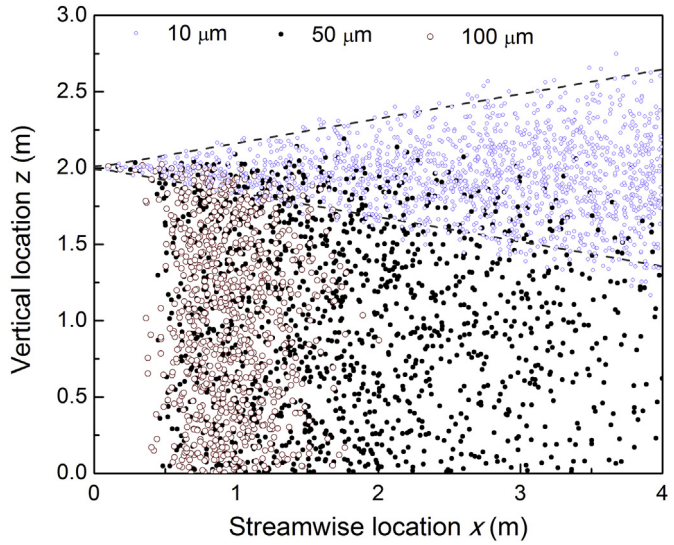

Fig. 5. Instantaneous dispersion pattern of particles (t = 100 s) in the buoyancy-neutral jet (mouth opening diameter D = 2 cm, initial velocity u_0 = 10 m/s, T_{amb} = 25°C). Particles are continuously released from t = 0. The top-hat width of the jet is indicated by the dashed line, which collapses with the visible boundary of the jet.

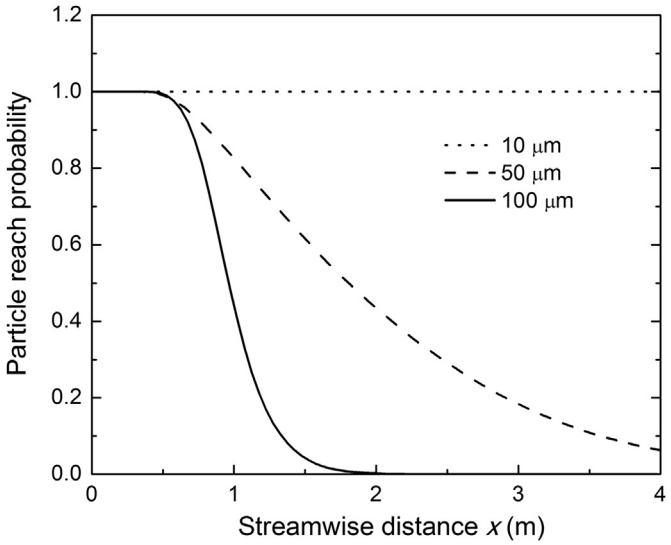

Fig. 7. Particle reach probability as a function of streamwise distance predicted by the DRW model. Trajectories of 50,000 particles were calculated in each case to improve the statistical reliability (mouth diameter$D$ = 2 cm, cough speed u_0 = 10 m/s, T_{amb} = 25 °C).

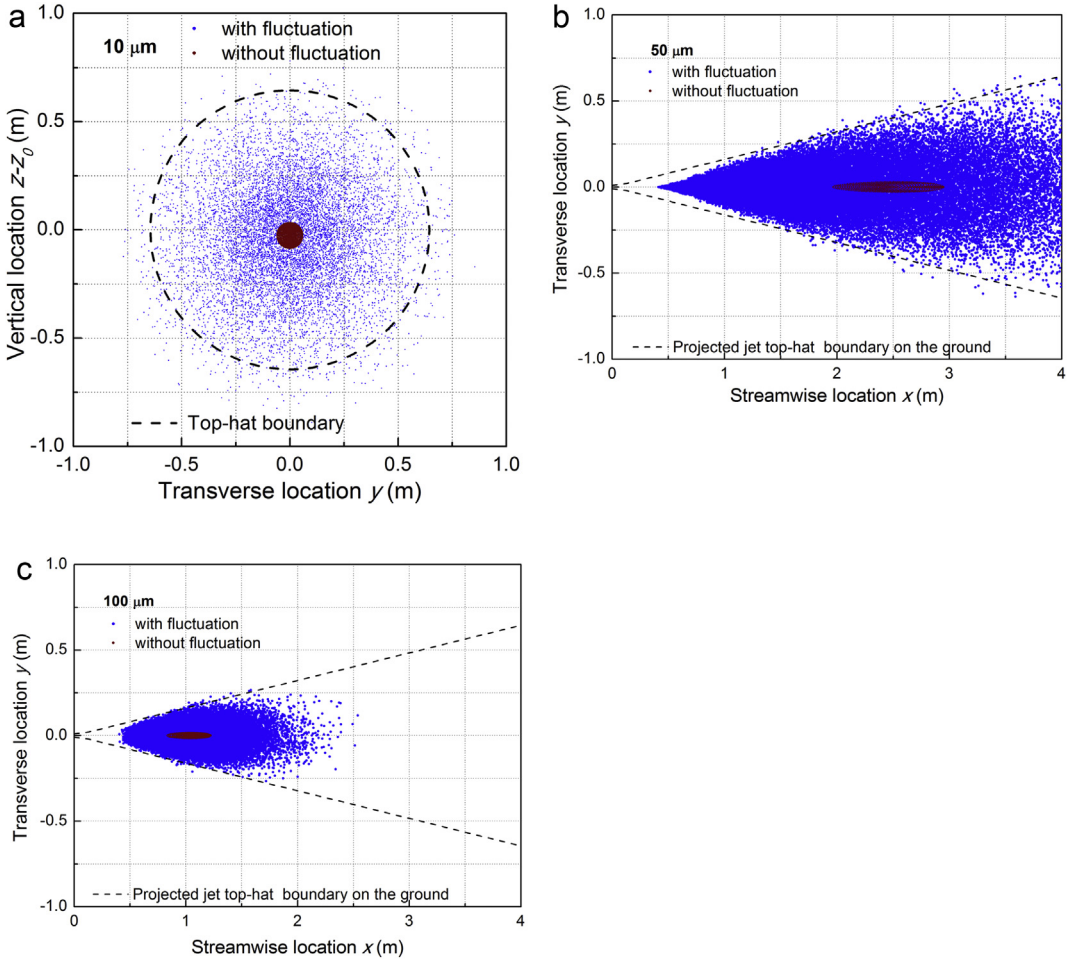

Fig. 6. Comparison of particle spread with (blue dots) and without (dark red dots) velocity fluctuation. (a) Particle position at x = 4 m for small particles (d_p = 10μm); (b,c) positions of the deposited particles on the ground (2 m below the nozzle) for medium (d_p = 50μm) and large particles (100 μm). Trajectories of 50,000 particles were calculated in each case to improve the statistical reliability (mouth diameter D = 2 cm, cough speed u_0 = 10 m/s, T_{amb} = 25 °C). (For interpretation of the references to colour in this figure legend, the reader is referred to the web version of this article.)

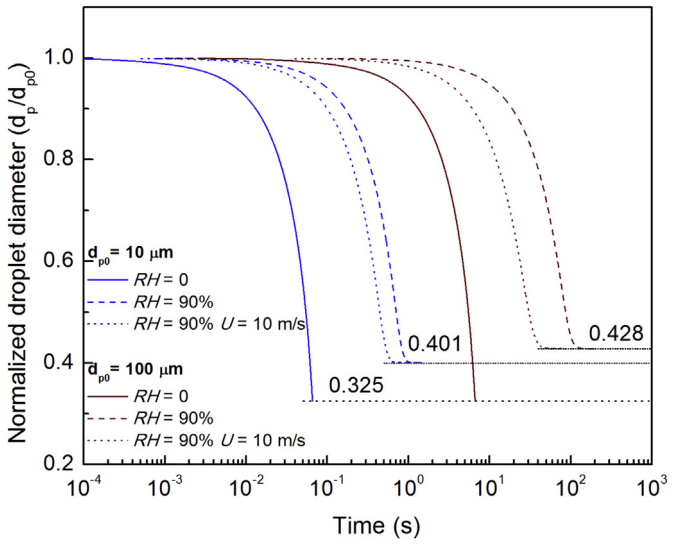

Fig. 8. Evaporation of droplets under different RH and relative velocity in air ($\Delta u = 0$ or 10 m/s). $d_{p0} = 10$ μm, blue line; $d_{p0} = 100$μm, dark red line. (For interpretation of the references to colour in this figure legend, the reader is referred to the web version of this article.)

wind tunnel. For each particle, its location was recorded by cameras as a function of time; some 800 examples of each type were recorded and averaged to yield the dispersion profiles in Fig. 3. Compared with the experimental results, the DRW predictions for the heaviest (glass and copper particles, error ≤20%) and lightest particles (hollow glass, error ≤ 15%) were reasonable, but were less reliable for the medium particles, e.g. corn pollen (error ≤ 47%). Small particles follow eddies until they dissipate, and large particles settle out of an eddy readily. However, medium particles are in between, and the DRW model has difficulty in precisely predicting the interaction time between medium particles and eddies.

3.2. Effect of homogeneous turbulence on particle settling

Numerical simulations were carried out to study the effect of homogeneous turbulent on particle settling. In this simulation, 500 particles were released from a height of 2 m (H) in a field of homogeneous turbulence and zero mean flow. The turbulence length scale is 0.09 m, and the velocity scale σ was varied to study its effect on particle settling. The time for a particle to fall 2 m was recorded, and the apparent settling velocity w_{sa} was calculated from

$$w_{sa} = H \Big/ \left(\frac{1}{N} \sum_{i=1}^{N} T_i \right) \tag{19}$$

where $N = 500$ is the particle number, T_i the deposition time.

predicted results from the DRW model (Fig. 4) show that curves of different particle sizes collapse for $0.1 < \sigma/w_s < 1$, and the discrepancy at strong turbulence may result from the non-linearity of drag force for large particles (d_p = 100μm) at high Re. Ford_p = 100μm (w_s = 0.246 m/s), when$|\mathbf{u_g} - \mathbf{u_p}| = 10w_s$,$Re$ = 15.8 and we obtain the drag coefficient $C_D = \frac{24}{\mathrm{Re}}(1 + 0.15\mathrm{Re}^{0.687}) = 3.04$ instead of$C_D = \frac{24}{\mathrm{Re}} = 1.52$, indicating that the non-linearity contributes 50% of the total drag force under this situation, according to Equation (2). Murray [51] obtained similar results in a water tank experiment by releasing 2 mm glass particles in a grid-generated turbulence field.

The DRW model predicts only a 5% reduction in settling velocity for small particles at$\sigma/w_s = 10$, while Nielsen [38] predicted it to be 20% with the continuous random walk (CRW) model. The CRW model creates a 'loitering effect' for settling particles by correlating velocity fluctuations withw_s; as a result, particles settle more slowly if there exits velocity fluctuation in the vertical direction.

3.3. Spread of particles in turbulent buoyancy-neutral jets

Only particles are considered here, without the effect of evaporation. The instantaneous dispersion pattern of particles at $t = 100$ s is shown in Fig. 5. Small particles followed the airflow closely and were dispersed in the whole jet region (marked by the top-hat half width, which collapsed with the visible jet boundary), while large ones seem not much affected by the airflow. They have ballistic trajectories and deposit not long after their release. Medium particles spread more widely, and some of them also deposited in the near-source region.

Most of the small particles travelled as far as 4 m, which was the uppermost boundary in our calculation, while larger ones tended to deposit. For statistical reliability, the positions of 50,000 small particles reaching x = 4 m and the deposition pattern of larger particles are shown in Fig. 6. Considering the distribution of the 10 μm particles at x = 4 m, without turbulence, the particles concentrated in a small circle of 0.06 m radius, which is slightly larger than the original 0.02 m, as compared with the spread diameter of 0.645 m (top-hat boundary) with turbulence. Note that the spread when there is no turbulence (shown in dark red dots in Fig. 6a) is achieved by the relatively small radial flow component (Equation (9)) close to the jet centre line. The particle release at the origin has no radial flow component. For medium particles, they begin to settle out of the jet and deposit from $x = 0.4$ m. The particle concentration in the jet decreases as it travels further; a portion of particles are able to reach x = 4 m. According to the predictions of the DRW model, particles of 100 μm can travel up to 2.5 m in the streamwise direction. Compared with the situation without velocity fluctuation (dark red dots in Fig. 6c), particles of a diameter of 100 μm are much more widely dispersed, e.g. for large particles, twice the maximum travelling distance (2.50 m compared with 1.23 m), a four-fold increase of the spread range in the streamwise direction x (from 0.40 m to 2.50 m, compared with 0.83~1.23 m), and a thirteen-fold increase of the dispersion range in the transverse direction y (−0.27~0.27 m, compared with −0.02~0.02 m). Hence with the presence of turbulence, the droplets spread much more in both streamwise and transverse directions. There is a greater spread distance in the streamwise direction (Fig. 6). This also agrees with Eames et al. [52], suggesting that it is important to fully consider the impact of turbulence in CFD studies of droplet dispersion in rooms.

The average settling velocity and the average streamwise travelling distance of 50,000 particles before deposition are shown in Table 2. It predicts a reduction in the average settling velocity, although it is not remarkable for 100 μm particles. The extremely high value of 32.9% for 50 μm particles predicted by the DRW model cannot result from the non-linearity of drag force, as revealed in 3.2. It is probably due to the vertical entrainment velocity; the entrainment velocity around the jet boundary is of the same scale as the terminal settling velocity of the medium particles (0.07 m/s) (Fig. 2). Because particles are widely dispersed in the DRW model, particularly near the jet nozzle, the average travelling distance is lower than that in the mean jet field.

One important question in the study of infection transmission is how far these respiratory particles or droplets could travel. The reach probability is defined as

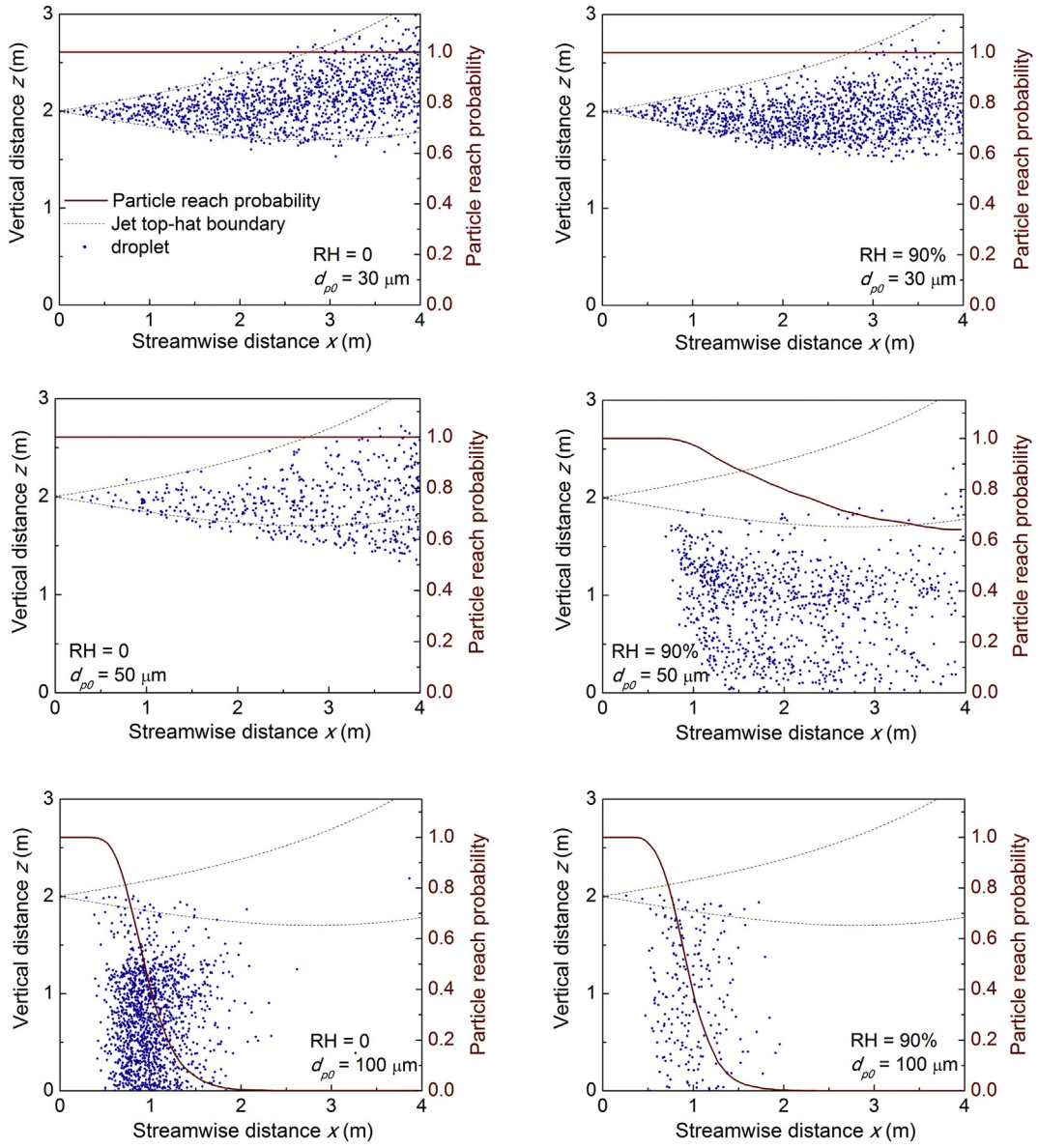

Fig. 9. Instantaneous distribution of droplets of different initial sizes (t = 50 s for 30 μm droplets; t = 200 s for 50 and 100 μm droplets) and their reach probability (dark red lines) in the turbulent buoyant jet (u_0 = 10 m/s, D = 2 cm). The effect of RH was studied by considering two humidity values: RH = 0 (left), RH = 90% (right). The temperature of exhaled airflow is 35.1 °C with the ambient temperature being 25 °C [53], and the cough airflow is saturated (RH = 100%). (For interpretation of the references to colour in this figure legend, the reader is referred to the web version of this article.)

$$p(x) = \frac{N_{Tot} - N_{Dep}(x)}{N_{Tot}} \tag{20}$$

where N_{Tot} and N_{Dep} are the total number of particles/droplets released and those that deposit before reaching a certain streamwise distance x, respectively.

Fig. 7 shows the particle reach probability for the cases in Fig. 6. Less than 10% of medium particles can travel further than 4 m, and only 1% of the 100 μm particles travel over 2 m, as predicted by the DRW model.

3.4. Effect of relative humidity and relative velocity on droplet evaporation

For the remainder of this paper, we include the effects of

Table 2
Comparison of the average settling velocity and the average travelling distance of 50,000 particles predicted by two models.

d_p (μm)	$\overline{w}_s$ without u' (m/s)	$\overline{w}_s$, with fluctuation (m/s)		$\overline{x}$ without u' (m)	$\overline{x}$, with fluctuation (m)	
		DRW (m/s)	Reduction (%)		DRW (m/s)	Reduction (%)
50	0.070	0.047	32.9	2.503	2.086	16.7
100	0.234	0.2305	1.5	1.073	1.021	4.8

evaporation. The evaporation process of a single droplet was first studied, as shown in Fig. 8. It takes 0.066 s and 6.63 s for droplets with initial sizes of 10 μm and 100 μm, respectively, to become droplet nuclei in still and dry conditions (RH = 0, and the relative velocity $\Delta u = 0$ m/s). The evaporation time here seems proportional to the square of the initial droplet diameter d_{p0}^2 (see Table 1 and Fig. 8). Similar results have been presented in other studies [18].

The ambient humidity has a significant effect on the evaporation rate of droplets, as the evaporation time increases to 1.52 s (23-fold) and 199.0 s (30-fold), respectively, in humid conditions (RH = 90%). Due to the Kelvin effect, small droplets have a smaller final normalised diameter (0.401) compared with large droplets (0.428), as shown in Fig. 8.

It is known that convection by a force velocity field increases the drying process; this effect is also remarkable, e.g. 1.03 s and 80.3 s are needed for droplets of 10 μm and 100 μm respectively to become droplet nuclei (RH = 90%,$\Delta u = 10$ m/s); however, this is not as significant as the effect of humidity, as discussed above. In addition, although the maximum coughing velocity could be more than 10 m/s, the relative velocity between air and droplets is usually much smaller.

3.5. Evaporative droplet spread in turbulent buoyant jets

Cough-expired air is usually warmer than ambient air, and the temperature difference decreases under hot conditions [53]. The difference in density creates a curved jet centreline, as indicated by Equation (12). Meanwhile, the exhaled air is saturated with lighter water vapour (it decreases the air density by 1.6% in extremely dry ambient conditions), but the higher CO_2 concentration increases the density by about 2%. The role of temperature difference is dominant, except at high ambient temperatures, e.g. 30 °C, when the role of RH becomes important (not shown, but can be easily estimated). For a cough jet at $T_{amb} = 5$°C and RH = 0, its centreline curves upward by 1.3 m when it reaches a streamwise distance of 4 m. Surely it will take small droplets with it, as already shown by Xie et al. [36]; we investigate how the fate of large droplets is affected.

Once expelled from the mouth, droplets begin to lose water and become droplet nuclei due to the water vapour pressure difference. Droplet nuclei are approximately a third of the initial size of droplets in dry conditions [9,17]. Our droplet evaporation model has been developed based on Liu's work.

In our numerical simulations, 5000 droplets were released, and three initial diameters of 30 μm, 50 μm, and 100 μm were investigated. Instantaneous droplet dispersion results (at $t = 50$ s for the 30 μm droplets, and 200s for the 50 μm and 100 μm droplets) are shown in Fig. 9. Droplets of initial size of 30 μm become droplet nuclei quickly in dry conditions (RH = 0), and then behave similarly to particles of 10 μm (Fig. 5), indicating the evaporation process is negligible In humid conditions (Fig. 9b), the droplet cloud shifts towards the lower jet boundary, but the difference compared with Fig. 5 is not obvious, and nearly all of the droplets travel further than 4 m.

The travelling distance of large droplets ($d_{p0} = 100$μm) seems unaffected by RH, e.g. the maximum travelling distance is over 2 m in two cases, because they settle out of the jet quickly in the near-source region (the settling velocity is 0.246 m/s for 100 μm droplets, Table 2) and don't evaporate completely until they reach the ground. However, there are more droplets depicted in Fig. 9e compared with Fig. 9f, because droplets that evaporate more slowly in humid conditions deposit more rapidly, thus having a shorter residence time in air. In addition, the upward curving airflow resulting from the temperature difference carries small droplets upwards, but this effect is negligible for large droplets, as seen in comparisons of the reach probability in Figs. 7 and 9e.

In contrast to small and large droplets, humidity has a remarkable effect on the dispersion of medium droplets (Fig. 9c and d). The settling velocity is 0.07 m/s for 50 μm droplets (Table 1) and it diminishes as droplets evaporate. It takes only 1–2 s for a medium droplet to shrink to a droplet nuclei (16.25 μm by our model) in dry conditions (RH = 0), and the evaporation is complete before they fall out of the jet. Droplet nuclei are small enough to follow the airflow closely and travel a considerable distance. However, in humid conditions, it takes nearly 30 times longer for droplets to reach their final size, so some of them deposit out of the jet around 1 m from the nozzle before becoming droplet nuclei. Since shrunken droplets settle slowly, some of them can be re-entrained into the jet, and the induced velocity outside the top-hat jet boundary is large enough to carry the droplets forward. In our calculations for the humid case, more than 60% of the medium droplets are able to travel 4 m, although it takes much longer than under dry conditions; under dry conditions, droplets nuclei stay close to the jet centreline, where there is a high streamwise velocity.

It is clear that the fate of small particles or droplets ($d_{p0} \leq 30$μm in our study) is mainly determined by the airflow itself, as they follow the airflow closely, and are not sensitive to RH. For medium droplets, we changed the boundary conditions (u_0 and D) and the ambient temperature at RH = 50%. Nearly all droplets could travel 4 m, although it takes longer at smaller u_0 and D. RH is the key parameter in determining their evaporation rate and thus whether they deposit or suspend. From this perspective, dry air could be key to the spread of infection, e.g. in aircraft, where the RH can be as low as 10% [54].

As shown in Fig. 10, there is an increasing ratio of droplets that deposit on the ground with increasing RH; droplet deposition becomes evident when RH ≥ 80%, which may be defined as the high humidity threshold for medium droplets here. Some 95% of the released droplets could be carried a distance of 4 m at RH = 80%, and only 64% at RH = 90%, indicating they are most sensitive to RH at higher RH. This is similar to the study on the evaporation of a single droplet by Liu et al. [17]. However, Chen and Zhao [16] came to a different conclusion; they reported the transient process from a droplet to a droplet nucleus due to evaporation can be ignored when the initial droplet diameter is less than 100 μm. Our detailed

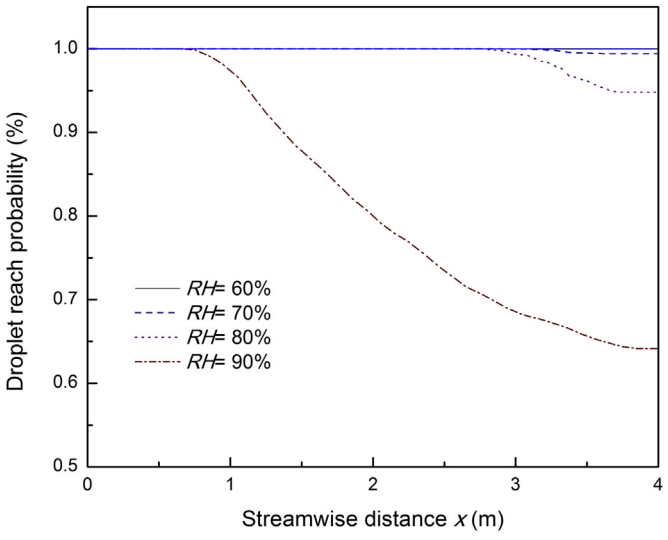

Fig. 10. Reach probability for droplets ($d_{p0} = 50$ μm). $T_{amb} = 25$°C, $u_0 = 10$ m/s, and $D = 2$ cm for all cases; RH was changed for the sensitivity study.

study revealed a different understanding. The impact of evaporation on the spread of medium sized droplets turns out to be the most significant. At the same time, the impact of evaporation on large droplets is not as important in terms of spread distance. The high RH condition is apparently an exception of the study by Chen and Zhao [16]. Large droplets remain in the large size range long enough to settle out of the jet, and RH is no longer the influential factor in terms of reach probability. Similarly, they are not sensitive to ambient temperature (not shown), although temperature alters the jet trajectory.

The sensitivity of the medium sized droplets (about 50 μm) reveals the importance of the number of droplet nuclei in airborne and large droplet transmission. The peak (mode) initial size for large droplets was found to be in the medium size range of 50–75 μm [9,55,56]. In dry conditions, these medium range droplets would dry out, become fine droplet nuclei, and contribute to airborne transmission. But in very humid conditions, they would maintain their diameter, and contribute to large droplet transmission following Wells [14]. At low RH, our results show that medium sized droplets (which happen to be the most numerous) would evaporate, drift along the air jet, and eventually become airborne. At high RH, they would evaporate at a slow rate, and be carried away by turbulence and the air jet, eventually falling out of the jet.

3.6. Limitations of this study

The focus of this study is the spread of exhaled droplets by a cough jet alone. A cough is a puff, rather than a jet. The dispersion of droplets in a puff may be different from that in a jet, so further study is still needed. However, the present model allowed us to study the impact of turbulence in a detailed manner. Another limitation of this study lies in ignoring the room airflows. There have been many studies of exhalation jet spread in the indoor environment, e.g. those by Qian et al. [19], Chao and Wan [49], Hang et al. [57]. In reality, when there are two or more people in close proximity, exhalation jets or puffs also interact. On the other hand, this is a worthwhile assumption as ignoring the complex room airflows allowed us to focus on the dispersion and spread of droplets by the cough jet alone. This expands upon the study of Klettner et al. [37] which focused on the homogenous turbulence, and did not consider the cough jet. In addition, the visualization of cough expired droplet trajectories by Bourouiba et al. [35] shows that droplets at the mouth exhibit a wide range of expiratory directions, rather than the uniform and iso-kinematic assumption in our study; components of saliva/mucus droplets are more complex, and the hygroscopicity of protein might decrease the evaporation rate of droplets [18].

4. Conclusion

The coughing airflow was represented as a turbulent jet to study the dispersion of expiratory droplets. The discrete random walk model was employed to study the effect of velocity fluctuation. Reach probability was defined to characterise the travelling distance of particles or droplets. This study shows that jet-like cough airflow prompts the wide spread of expiratory droplets and that the effect of evaporation on medium droplets (50 μm) is significant.

Particles are widely dispersed in the presence of velocity fluctuation. Small droplets follow the airflow closely. They are dispersed in the whole jet region, and are carried a long distance, while only 1% of large ones (e.g. 100 μm) will be transported over 2 m by a typical cough jet ($u_0 = 10$ m/s, $D = 2$ cm). Although the presence of turbulence would increase the residence time, in particular for large particles, the entrainment of a jet is more significant in suspending the smaller particles for a longer period before they deposit. For large droplets, there is a four-fold increase in the dispersion range in the streamwise x direction, and a thirteen-fold increase in the dispersion range in transverse y direction compared with that with no fluctuation.

Small droplets ($d_{p0} = 30$ μm) are not sensitive to relative humidity (RH) and become droplet nuclei soon after being expired, and then behave similarly to small particles (10 μm). Medium droplets are very sensitive to RH under humid conditions (threshold value RH $\geq$ 80%), when they settle out of the jet but deposit slowly, and are thus carried forward in the jet-induced velocity field. Nearly 95% are carried a distance of 4 m at RH = 80%, and only 60% at RH = 90%, indicating they are most sensitive to RH at higher RH. The travelling distance of large droplets is mainly determined by the jet outlet boundary. Their maximum travelling distance almost doubles if the jet outlet velocity or diameter is doubled. Varying ambient temperature or humidity doesn't influence the reach probability function of large droplets significantly.

Acknowledgements

This study was funded by a RGC General Research Fund by RGC (HKU7142/12) and a NSFC fund (51278440). We would also like to thank Professor Joseph H.W. Lee and Dr Shu Ning Chan for their help in building and evaluating the particle dispersion model.

References

[1] G. Brankston, L. Gitterman, Z. Hirji, C. Lemieux, M. Gardam, Transmission of influenza A in human beings, Lancet Infect. Dis. 7 (4) (2007) 257–265.
[2] R. Tellier, Review of aerosol transmission of Influenza A virus, Emerg. Infect. Dis. (2006) 121657–121662.
[3] T.P. Weber, N.I. Stilianakis, Inactivation of influenza A viruses in the environment and modes of transmission: A critical review, J. Infect. 57 (5) (2008) 361–373.
[4] B.B. Ross, R. Gramiak, H. Rahn, Physical Dynamics of the Cough Mechanism, J. Appl. Physiol. 8 (3) (1955) 264–268.
[5] M. Vasudevan, C.F. Lange, Property dependence of onset of instability in viscoelastic respiratory fluids, Int. J. Eng. Sci. 43 (15–16) (2005) 1292–1298.
[6] M. Vasudevan, C.F. Lange, Surface tension effects on instability in viscoelastic respiratory fluids, Math. Biosci. 205 (2) (2007) 180–194.
[7] L. Morawska, Droplet fate in indoor environments, or can we prevent the spread of infection? Indoor Air 16 (5) (2006) 335–347.
[8] H. Holmgren, E. Ljungstrom, Influence of film dimensions on film droplet formation, J. Aerosol Med. Pulm. Drug Deliv. 25 (1) (2012) 47–53.
[9] J.P. Duguid, The size and the duration of air-carriage of expiratory droplets and droplet-nuclei, J. Hyg. 44 (1946) 471–479.
[10] R.S. Papineni, F.S. Rosenthal, The size distribution of droplets in the exhaled breath of healthy human subjects, J. Aerosol Med. 10 (2) (1997) 105–116.
[11] R.G. Loudon, R.M. Roberts, Cough frequency in patients with respiratory disease, Am. Rev. Resp. Dis. 96 (1967) 1137–1143.
[12] S.H. Yang, G.W.M. Lee, C.M. Chen, C.C. Wu, K.P. Yu, The size and concentration of droplets generated by coughing in human subjects, J. Aerosol Med. Depos. Clear. Eff. Lung 20 (4) (2007) 484–494.
[13] C.Y.H. Chao, M.P. Wan, L. Morawska, G.R. Johnson, Z.D. Ristovski, et al., Characterization of expiration air jets and droplet size distributions immediately at the mouth opening, J. Aerosol Sci. 40 (2) (2009) 122–133.
[14] W.F. Wells, On air-borne infection study: II—droplets and droplet nuclei, Am. J. Epidemiol. 20 (3) (1934) 611–618.
[15] W.G. Lindsley, F.M. Blachere, R.E. Thewlis, A. Vishnu, K.A. Davis, et al., Measurements of airborne influenza virus in aerosol particles from human coughs, PLoS ONE 5 (11) (2010).
[16] C. Chen, B. Zhao, Some questions on dispersion of human exhaled droplets in ventilation room: answers from numerical investigation, Indoor Air 20 (2) (2010) 95–111.
[17] L. Liu, J.J. Wei, Y.G. Li, A. Ooi, How exhaled droplets become droplet nuclei, and their dispersion as a function of composition and humidity, 2015. Submitted for Revision.
[18] J. Redrow, S.L. Mao, I. Celik, J.A. Posada, Z.G. Feng, Modeling the evaporation and dispersion of airborne sputum droplets expelled from a human cough, Build. Environ. 46 (10) (2011) 2042–2051.
[19] H. Qian, Y. Li, P.V. Nielsen, C.E. Hyldgaard, T.W. Wong, et al., Dispersion of exhaled droplet nuclei in a two-bed hospital ward with three different ventilation systems, Indoor Air 16 (2) (2006) 111–128.
[20] Y. Li, G.M. Leung, J.W. Tang, X. Yang, C.Y.H. Chao, et al., Role of ventilation in

airborne transmission of infectious agents in the built environment – a multidisciplinary systematic review, Indoor Air 17 (1) (2007) 2–18.
[21] P.V. Nielsen, Control of airborne infectious diseases in ventilated spaces, J. R. Soc. Interface 6 (Suppl. 6) (2009) S747–S755.
[22] R.P. Clark, O.G. Edholm, Man and His Thermal Environment, Arnold, London, 1985.
[23] S. Murakami, Analysis and design of micro-climate around the human body with respiration by CFD, Indoor Air (2004) 14144–14156.
[24] N.P. Gao, J.L. Niu, CFD study of the thermal environment around a human body: A review, Indoor Built Environ. 14 (1) (2005) 5–16.
[25] B.A. Edge, E.G. Paterson, G.S. Settles, Computational study of the wake and contaminant transport of a walking human, J. Fluids Eng. 127 (5) (2005) 967–977.
[26] J.I. Choi, J.R. Edwards, Large-eddy simulation of human-induced contaminant transport in room compartments, Indoor Air 22 (1) (2012) 77–87.
[27] J.W. Tang, I. Eames, Y. Li, Y.A. Taha, P. Wilson, et al., Door-opening motion can potentially lead to a transient breakdown in negative-pressure isolation conditions: the importance of vorticity and buoyancy airflows, J. Hosp. Infect. 61 (4) (2005) 283–286.
[28] ASHRAE, Thermal Environmental Conditions for Human Occupancy, American Society of Heating, Refrigerating and Air-Conditioning Engineers (ANSI/ASHRAE Standard 55-2004), Atlanta, 2004.
[29] J.K. Gupta, C.H. Lin, Q. Chen, Flow dynamics and characterization of a cough, Indoor Air 19 (6) (2009) 517–525.
[30] S.B. Kwon, J. Park, J. Jang, Y. Cho, D.S. Park, C. Kim, A. Jang, Study on the initial velocity distribution of exhaled air from coughing and speaking, Chemosphere 87 (11) (2012) 1260–1264.
[31] A.M.D. Hasan, C.F. Lange, M.L. King, Effect of artificial mucus properties on the characteristics of airborne bioaerosol droplets generated during simulated coughing, J. Newt. Fluid Mech. 165 (21–22) (2010) 1431–1441.
[32] S. Zhu, S. Kato, J.-H. Yang, Study on transport characteristics of saliva droplets produced by coughing in a calm indoor environment, Build. Environ. 41 (12) (2006) 1691–1702.
[33] J.W. Tang, T.J. Liebner, B.A. Craven, G.S. Settles, A schlieren optical study of the human cough with and without wearing masks for aerosol infection control, J. R. Soc. Interface 6 (Suppl. 6) (2009) S727–S736.
[34] M. Vansciver, S. Miller, J. Hertzberg, Particle Image Velocimetry of Human Cough, Aerosol Sci. Technol. 45 (3) (2011) 415–422.
[35] L. Bourouiba, E. Dehandschoewercker, J.W.M. Bush, Violent expiratory events: on coughing and sneezing, J. Fluid Mech. 745 (2014) 537–563.
[36] X. Xie, Y. Li, A.T.Y. Chwang, P.L. Ho, W.H. Seto, How far droplets can move in indoor environments – revisiting the Wells evaporation–falling curve, Indoor Air 17 (3) (2007) 211–225.
[37] C.A. Klettner, I. Eames, J.W. Tang, The effect of turbulence on the spreading of infectious airborne droplets in hospitals. New Approaches in Modeling Multiphase Flows and Dispersion in Turbulence, Fractal Methods and Synthetic Turbulence, ERCOFTAC Ser. 18 (2012) 141–152.
[38] P. Nielsen, Coastal bottom boundary layers and sediment transport, in: Advanced Series on Ocean Engineering, vol. 4, World Scientific, 1992.
[39] J.H.W. Lee, V.H. Chu, Turbulent Jets and Plumes: a Lagrangian Approach, Kluwer Academic Publishers, Boston, 2003.
[40] S.N. Chan, Ken W.Y. Lee, Joseph H.W. Lee, Numerical modelling of horizontal sediment-laden jets, Environ. Fluid Mech. 14 (2014) 173–200.
[41] A.D. Gosman, E. Ioannides, Aspects of computer-simulation of liquid-fueled combustors, J. Energy 7 (6) (1983) 482–490.
[42] J. Kukkonen, T. Vesala, M. Kulmala, The interdependence of evaporation and settling for airborne freely falling droplets, J. Aerosol Sci. 20 (1989) 749–763.
[43] W.C. Hinds, Aerosol Technology: Properties, Behavior, and Measurement of Airborne Particles, second ed., J. Wiley, New York, 1999.
[44] W.A. Sirignano, Fluid Dynamics and Transport of Droplets and Sprays, Cambridge University Press, Cambridge, 1999.
[45] V.V. Baturin, Fundamentals of Industrial Ventilation, Pergamon Press, Oxford, 1972.
[46] H.B. Fischer, E.J. List, R.C.Y. Koh, J. Imberger, N.H. Brooks, Mixing in Inland and Coastal Waters, 1979.
[47] W. Rodi, Turbulent Buoyant Jets and Plume, Pergamon Press, Oxford, 1982.
[48] C.J. Chen, W. Rodi, Vertical Turbulent Buoyant Jets - A Review of Experimental Data, Pergamon Press, London, UK, 1980, pp. 15–48.
[49] C.Y.H. Chao, M.P. Wan, A study of the dispersion of expiratory aerosols in unidirectional downward and ceiling-return type airflows using a multiphase approach, Indoor Air 16 (4) (2006) 296–312.
[50] W.H. Snyder, J.L. Lumley, Some measurements of particle velocity autocorrelation functions in a turbulent flow, J. Fluid Mech. 48 (1971) 41–71.
[51] S.P. Murray, Settling velocities and vertical diffusion of particles in turbulent water, J. Geophys. Res. 75 (9) (1970) 1647–1654.
[52] I. Eames, D. Shoaib, C.A. Klettner, V. Taban, Movement of airborne contaminants in a hospital isolation room, J. R. Soc. Interface 6 (Suppl. 6) (2009) S757–S766 rsif20090319.
[53] P. Hoppe, Temperatures of expired air under varying climatic conditions, Int. J. Biometeorol. 25 (2) (1981) 127–132.
[54] E.H. Hunt, D.H. Reid, D.R. Space, F.E. Tilton, Commercial airliner environmental control system – engineering aspects of cabin air quality, Proc. Annu. Meet. Aerosp. Med. Assoc. (1995) 1–8.
[55] J.F. Duguid, The numbers and the sites of origin of the droplets expelled during expiratory activities, Edinbg. Med. J. 52 (1945) 335–340.
[56] X. Xie, Y. Li, H.Q. Sun, L. Liu, Exhaled droplets due to talking and coughing, J. R. Soc. Interface 6 (2009) 703–714.
[57] J. Hang, Y. Li, R. Jin, The influence of human walking on the flof and airborne transmission in a six-bed isolation room: tracer gas simulation, Build. Environ. 77 (2014) 119–134.